NANO LETTERS

2006
Vol. 6, No. 10
2191−2195

Impact Ionization Can Explain Carrier Multiplication in PbSe Quantum Dots

A. Franceschetti,* J. M. An, and A. Zunger

National Renewable Energy Laboratory, Golden, Colorado 80401

Received May 31, 2006; Revised Manuscript Received August 10, 2006

ABSTRACT

The efficiency of conventional solar cells is limited because the excess energy of absorbed photons converts to heat instead of producing electron–hole pairs. Recently, efficient carrier multiplication has been observed in semiconductor quantum dots. In this process, a single, high-energy photon generates multiple electron–hole pairs. Rather exotic mechanisms have been proposed to explain the efficiency of carrier multiplication in PbSe quantum dots. Using atomistic pseudopotential calculations, we show here that the more conventional impact ionization mechanism, whereby a photogenerated electron–hole pair decays into a biexciton in a process driven by Coulomb interactions between the carriers, can explain both the rate (≪1 ps) and the energy threshold (∼2.2 times the band gap) of carrier multiplication, without the need to invoke alternative mechanisms.

Solar cells are a source of clean, sustainable energy, but to make them competitive with fossil fuels their efficiency must be increased significantly.[1] A major drawback of conventional solar cells is that high-energy photons at the blue end of the solar spectrum are largely wasted because their excess energy $\hbar\omega - E_g$ (where ω is the photon frequency and E_g is the solar-cell band gap) is converted into heat by electron−phonon scattering processes, instead of being used to produce additional electron−hole pairs. This efficiency bottleneck could be overcome by direct carrier multiplication.[2−10] In this process, a *single* absorbed high-energy photon generates *two or more* electron−hole pairs, thereby potentially increasing the output electrical current of the solar cell. In *bulk solids*, direct carrier multiplication is rather inefficient because competing decay channels for the photogenerated electron−hole pairs, such as phonon-assisted electron/hole cooling, are extremely fast. For example, in crystalline Si solar cells a maximum carrier multiplication efficiency of 30% at $\hbar\omega = 4.6$ eV was reported,[11] meaning that on average one photon generates 1.3 excitons. In *quantum dots*, dramatically higher carrier multiplication efficiencies have been observed recently.[5−9] For example, Schaller et al.[8] reported quantum efficiencies as high as 700% in PbSe colloidal nanocrystals. However, the mechanism of carrier multiplication in quantum dots is still unknown.

In bulk solids, carrier multiplication can occur through a scattering mechanism known as impact ionization (II).[12,13] In this process (Figure 1), a photon of energy $\hbar\omega > 2E_g$ creates a highly excited electron−hole pair, which in turn decays into a biexciton through an energy-conserving transition driven by many-body Coulomb interactions between carriers. However, II was dismissed[6,7] as a possible explanation of carrier multiplication in PbSe quantum dots on the basis that it would be too slow to account for the observed high carrier multiplication efficiency. Instead, rather exotic explanations, involving resonance between single-exciton and multi-exciton states,[6] or second-order coupling with virtual excitons,[7] were tentatively offered. Indeed, pseudopotential calculations[3,4] of the II rate in CdSe quantum dots at threshold ($\hbar\omega \approx 2E_g$) predicted a II lifetime $\tau^{II} = 76$ ps, which is too slow to explain efficient carrier multiplication. However, the II rate at higher energy ($\hbar\omega > 2E_g$) was not calculated. Recent tight-binding calculations[14] have suggested that the II rate at a given exciton energy is similar in PbSe quantum dots and in bulk PbSe. In this Letter we show, via atomistic pseudopotential calculations of the electronic structure of PbSe quantum dots, that the II mechanism can indeed explain the observed carrier multiplication lifetime and energy threshold. This different interpretation could lead to different optimization strategies for high-efficiency solar cells.

The experimental observation of carrier multiplication in quantum dots[5−9] has raised several interesting questions:

(i) *Asymmetry between carrier multiplication and Auger recombination rates*: Carrier multiplication was shown[6,7] to have a much shorter lifetime than the nonradiative decay of a biexciton into a single-exciton (Auger recombination, AR). The II decay rate of an exciton state $|X_i\rangle$, of energy E_i is given, according to the Fermi golden rule, by

$$\frac{1}{\tau_i^{II}} = \frac{2\pi}{\hbar}\sum_f |\langle X_i|W|XX_f\rangle|^2 \delta(E_i - E_f) \qquad (1)$$

where the sum runs over the biexciton states $|XX_f\rangle$ of energy E_f and W is the screened Coulomb interaction.[15] Conversely, the AR decay rate of a biexciton is given by

$$\frac{1}{\tau_i^{AR}} = \frac{2\pi}{\hbar}\sum_f |\langle XX_i|W|X_f\rangle|^2 \delta(E_i - E_f). \qquad (2)$$

* Corresponding author. E-mail: alberto_franceschetti@nrel.gov.

10.1021/nl0612401 CCC: $33.50
Published on Web 09/08/2006

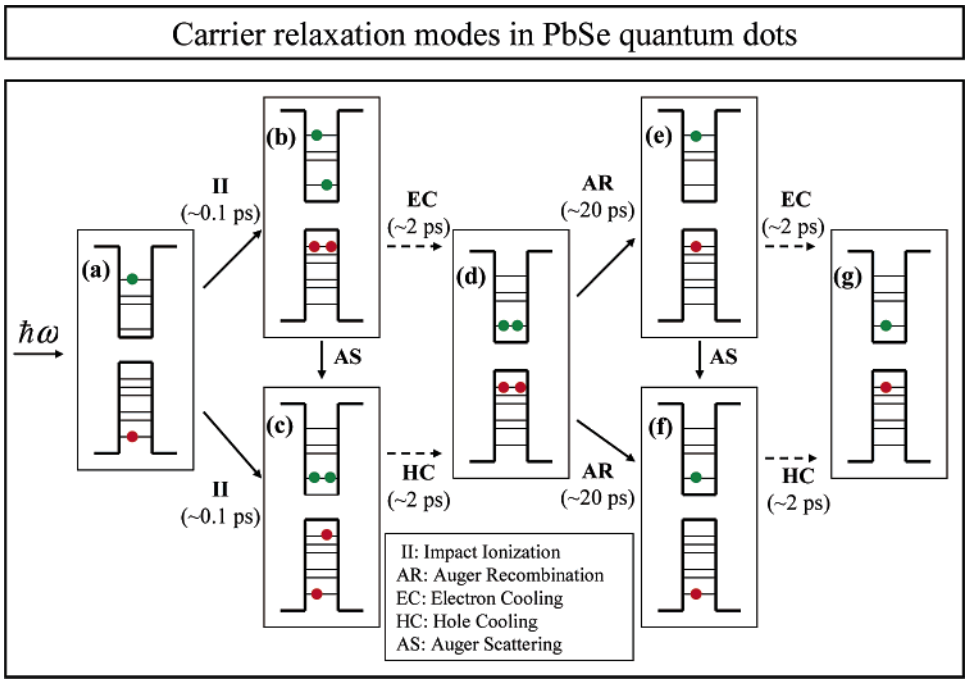

Figure 1. Schematic diagram of the processes discussed in this work. In the impact ionization process, a photogenerated electron−hole pair (a) creates two electron−hole pairs (b and c). The two electrons and the two holes can then relax nonradiatively, e.g. via phonon emission (electron/hole cooling), to form a ground-state biexciton (d). The biexciton decays into an excited single exciton (e and f) via Auger recombination. Finally, the single exciton thermalizes via electron/hole cooling (g). Solid arrows denote energy-conserving processes, while dashed arrows denote dissipative processes. Electrons are shown in green, and holes are shown in red.

Thus, the II and AR processes are described by the same transition matrix elements $\langle X|W|XX\rangle$. The observation of a highly *asymmetric* transition probability, whereby carrier multiplication is much faster than Auger recombination, has led to suggestions[6,7] that II cannot explain carrier multiplication in PbSe quantum dots. Ellingson et al.[6] proposed that a photon of energy $\hbar\omega > 2E_g$ creates a *coherent* superposition of degenerate single-exciton (Figure 1a) and multi-exciton (Figure 1b and c) states, coupled by interparticle Coulomb interactions. The efficiency of the multi-exciton generation process is due to the different dephasing rates of single- and multi-excitons.[6] Schaller et al.[7] proposed instead a second-order perturbative process, whereby a single absorbed photon generates a biexciton instantaneously, via coupling with virtual single-exciton states. Thus, the mechanism of carrier multiplication in PbSe quantum dots remains an open question.

(ii) *Carrier multiplication threshold*: Significantly different values of the energy threshold $\hbar\omega_{th}$ for carrier multiplication, that is, the minimum photon energy necessary to achieve multi-exciton generation, have been reported in the literature. Schaller et al. observed a threshold of $\hbar\omega_{th} \approx 3E_g$ in PbSe quantum dots 4−6 nm in diameter,[5,7−9] whereas Ellingson et al.[6] observed a threshold of $\hbar\omega_{th} \approx 2.1E_g$ in PbSe quantum dots 3.9−5.4 nm in diameter. Schaller et al.[5,8] rationalized their observed $\sim 3E_g$ threshold by suggesting that because PbSe has similar electron and hole effective masses, the electron and hole energy levels would have approximately the same spacing, leading to a "mirrorlike" symmetry of valence and conduction states[16]. Ellingson et al.[6] argued that their reported $2.1E_g$ threshold can be explained by assuming that parity-forbidden transitions (e.g., P → S or S → P) are in fact optically allowed. However, it was shown recently[17] that the assumed mirrorlike symmetry between valence and conduction levels does not exist and S-to-P transitions are forbidden. Thus, the exact carrier-multiplication threshold, and what controls it, is still undetermined.

Here we use accurate atomistic pseudopotential methods to address these controversial findings. We find that (i) the observed asymmetry between the II and AR transition rates is due to the very different densities of final states for these processes. The II rate overcomes the AR rate already at $2.1E_g$ and becomes at least 2 orders of magnitude faster at $3E_g$. We also find that (ii) the II threshold is $\hbar\omega \approx 2.2E_g$, in agreement with the experimental results of ref 6, but in disagreement with their model. We show that the $\sim 2.2E_g$ threshold is due to the lack of mirrorlike symmetry between valence and conduction states, not to optically forbidden transitions. Our results suggest that the II mechanism can explain carrier multiplication in quantum dots and that alternative explanations[6,7] are not needed.

The relevant decay processes are summarized in Figure 1. When a photon of energy $\hbar\omega > 2E_g$ is absorbed by a quantum dot, it creates a high-energy electron hole pair (Figure 1a), which can then decay into a biexciton via II (Figure 1b and c). The biexciton will then relax to its ground state via phonon-assisted electron cooling (EC) and/or hole cooling (HC) processes, which can be facilitated by electron−hole Auger scattering (AS).[15,18] Typical cooling times in PbSe quantum dots are <10 ps. The primary decay channel for ground-state biexcitons (Figure 1d) is by Auger recombination ($\tau^{AR} \approx 20$ ps), which leads to excited mono-exciton

states (Figure 1e and f). Finally, the electron and the hole relax via electron/hole cooling, leading to a ground-state exciton (Figure 1g). In this Letter, we focus on the II and AR processes.

We consider a nearly spherical $Pb_{260}Se_{249}$ quantum dot 3.1 nm in diameter. The dot is obtained by cutting out a Se-centered sphere from bulk PbSe (rocksalt lattice structure, lattice constant $a_0 = 6.12$ Å). All Pb and Se surface atoms are passivated using ligand-like atomic pseudopotentials (centered along the direction of the dangling bonds), that are fitted to remove surface states from the dot band gap. The single-particle energies, ϵ_i, and wave functions, ψ_i, are then obtained by solving the single-particle Schrödinger equation

$$\left[-\frac{\hbar^2}{2m}\nabla^2 + V(\boldsymbol{r}) + \hat{V}_{\mathrm{SO}}\right]\psi_i(\boldsymbol{r}) = \epsilon_i\psi_i(\boldsymbol{r}) \qquad (3)$$

where $\hat{V}_{\mathrm{SO}}$ is the nonlocal spin−orbit operator and $V(\boldsymbol{r}) = \sum_{\boldsymbol{R}} v(\boldsymbol{r} - \boldsymbol{R})$ is a linear superposition of screened atomic pseudopotentials centered at the atomic positions $\{\boldsymbol{R}\}$. The Pb and Se atomic pseudopotentials are fitted to bulk PbSe transition energies and effective masses.[17] Equation 3 is solved by expanding the wave functions $\psi_i(\boldsymbol{r})$ in a plane-wave basis set. We calculate all of the valence states and the conduction states in an energy window of ∼5 eV above the band gap, for a total of ∼2000 single-particle states. Our pseudopotential approach fully includes inter-valley coupling as well as inter-band coupling, both arising from the finite size of the quantum dot and the lack of translational symmetry.

Figure 2a shows the single-particle density of states (DOS) of the 3.1 nm quantum dot, calculated from eq 3. The band gap is $E_g = 1.6$ eV. The most striking feature of the DOS is the very dense manifold of valence states, which form a quasi-continuum of levels near the valence-band edge. We find that the proposed mirrorlike symmetry between valence and conduction states, predicted by 8 × 8 **k·p** calculations,[16] does not exist in a realistic atomistic pseudopotential calculation. This is a result of (i) the presence of valence states originating from multiple valleys in the Brillouin zone, located along the L−K and K−X lines, which are not included in **k·p** calculations,[16] and (ii) the existence of a finite potential barrier at the surface of the dot, which leads to a more densely spaced manifold of valence-band energy levels compared to the case of an infinite potential barrier. Figure 2b shows densities of states of the mono-exciton (X) and the bi-exciton (XX), calculated as $\rho_X(E) = \sum_f \delta(E - E_f^X)$ and $\rho_{XX}(E) = \sum_f \delta(E - E_f^{XX})$, respectively. The mono-exciton and bi-exciton energies are evaluated here without interparticle Coulomb and exchange interactions, that is, $E(X_{v,c}) = \epsilon_c - \epsilon_v$, and $E(XX_{v,c,v',c'}) = \epsilon_c - \epsilon_v + \epsilon_{c'} - \epsilon_{v'}$, where $\epsilon_v(\epsilon_c)$ are the valence (conduction) single-particle energy levels. This is a good approximation in PbSe, where the large dielectric constant ($\epsilon_\infty = 23$) effectively screens interparticle interactions. The X and XX DOS's threshold (defined as the energies below which the DOS vanishes) are E_g and $2E_g$, respectively. Interestingly, we find that although

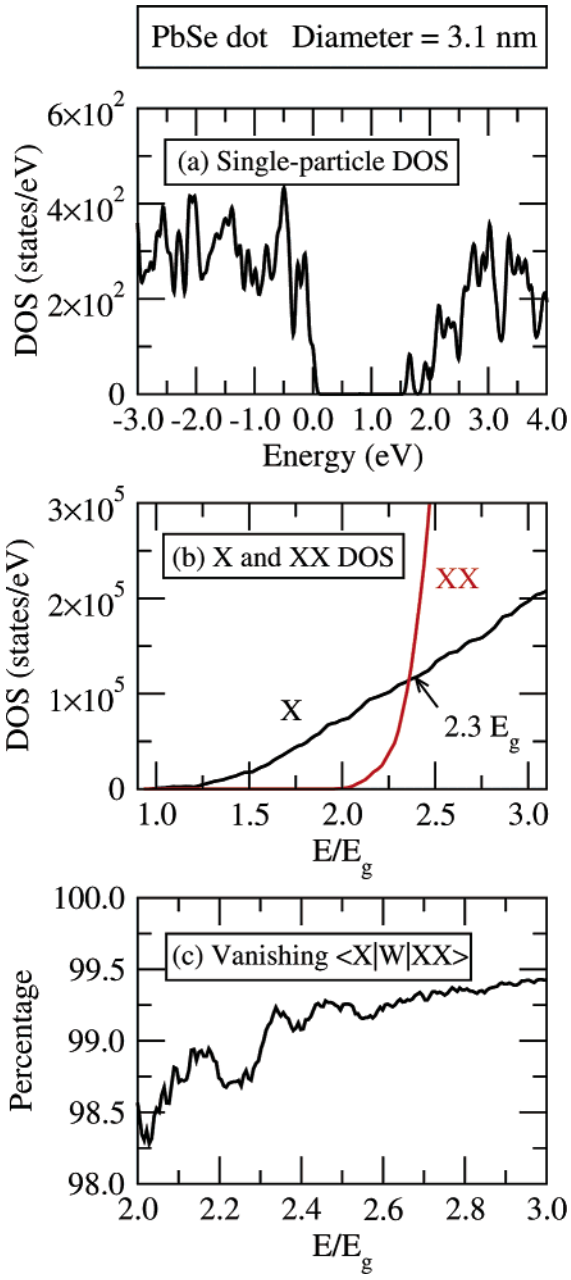

Figure 2. (a) Calculated single-particle density of states of a PbSe quantum dot 3.1 nm in diameter. The energy zero corresponds to the valence-band maximum. (b) shows the calculated single-exciton (X) and bi-exciton (XX) densities of states of the same quantum dot, as a function of the renormalized energy E/E_g, where E_g is the single-particle band gap of the quantum dot (1.6 eV). The DOS's have been broadened by a 50 meV Gaussian. The fraction of transition matrix elements $\langle X|W|XX\rangle$ that vanish due to the Coulomb selection rule is shown in part (c) as a function of the renormalized energy E/E_g.

the X DOS scales approximately linearly with energy in the interval $2E_g < E < 3\ E_g$, the XX DOS scales as $\rho_{XX}(E) \propto (E - 2E_g)^5$. The reason is that the number of ways of distributing the energy between two excitons increases much more rapidly, as a function of energy, than the number of single exciton states. As a result, the X and XX DOS's intersect at some energy, which in the case of a 3.1 nm quantum dot is 2.35 E_g (Figure 2b).

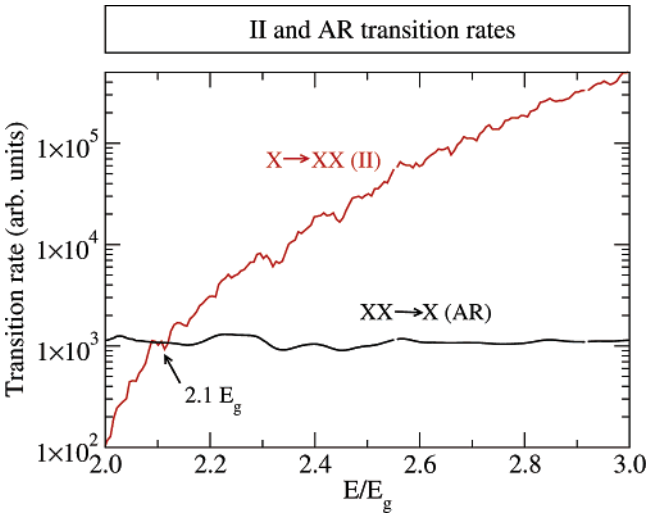

Figure 3. II and AR rates of a PbSe quantum dot 3.1 nm in size as a function of the renormalized energy E/E_g. The final states have been broadened by a 50 meV Gaussian. Note the crossover between the II and AR rates around $2.1E_g$.

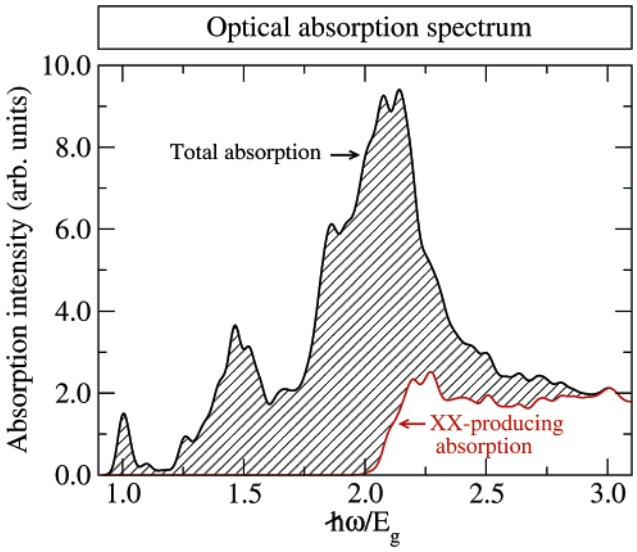

Figure 4. Optical absorption spectrum of a PbSe quantum dot 3.1 nm in size (black solid line), as a function of the renormalized photon energy $\hbar\omega/E_g$. Also shown is the part of the absorption spectrum contributing to II (red solid line).

Figure 2b reveals the existence of very different densities of final states for the II and AR processes of eqs 1 and 2, suggesting the possibility of different transition rates. However, the density of final states is not by itself a reliable indicator of the actual II and AR transition rates, because some transition matrix elements in eqs 1 and 2 may vanish as a consequence of the selection rules enforced by the two-particle character of the Coulomb interaction. For example, to first order the II process can occur only if one of the two electrons (or one of the two holes) in the final XX configuration occupies the same single-particle level as the electron (or the hole) in the initial X configuration (see Figure 1). Figure 2c shows that indeed a large fraction (>98%) of the transition matrix elements $\langle X|W|XX\rangle$ vanish as a result of this many-body selection rule. Thus, it is important to take into account the existence of many-body forbidden transitions to obtain accurate estimates of the II and AR rates.

We have calculated the II and AR rates by identifying the transition matrix elements that are zero (many-body forbidden), and assuming that the non-zero matrix elements are approximately constant. We have averaged the II and AR rates over the initial states in a narrow energy window (20 meV), to account for (i) the electronic dephasing of the initial state, which we assume to occur on a very fast time scale, and (ii) the statistical nature of ensemble measurements. The ensuing transition rates are shown in Figure 3. Remarkably, we find that the AR rate (XX → X) is almost constant as a function of energy. This is a consequence of the fact that the nearly linear increase of the density of final states (X) with energy (Figure 2b) is compensated by the increasing fraction of transition matrix elements that vanish (Figure 2c). The II rate (X → XX), however, increases rapidly with energy, overtaking the AR rate already at $\sim 2.1E_g$ (Figure 3). For $\hbar\omega = 3E_g$, we find that the II rate is over 2 orders of magnitude faster than the AR rate, thus explaining the observed[5,6] asymmetry between AR and II lifetimes.

The II lifetime can be estimated from the calculated ratio between the II and AR rates (Figure 3). The experimental AR lifetime (extrapolated to the size of the PbSe dot considered here) is approximately 6 ps,[5] which gives, from our calculations, an estimated II lifetime $\tau^{II} \approx 0.01$ ps at $\hbar\omega = 3E_g$. Using this value of τ^{II}, we can extract from eq 1 and Figure 3 the average value of the nonvanishing matrix elements $\langle X|W|XX\rangle$, which is ~0.2 meV. The experimental AR lifetime increases almost linearly with the nanocrystal volume,[5] whereas the ratio between the II and AR lifetimes at a given $\hbar\omega/E_g$ is expected to remain approximately constant. For a 6 nm PbSe quantum dot, we estimate that $\tau^{II} \approx 0.1$ ps at $\hbar\omega = 3E_g$. Thus, the II model of eq 1 appears to explain existing experimental observations[5−9] of ultrafast carrier multiplication in PbSe quantum dots for $\hbar\omega \geq 3E_g$. Interestingly, we also find that at low excitation energies ($\hbar\omega \approx 2E_g$), τ^{II} is approximately 10 times *slower* than τ^{AR} (see Figure 3). Using the value $\tau^{AR} \approx 6$ ps, we obtain $\tau^{II} \approx 60$ ps at $\hbar\omega \approx 2E_g$. This result is qualitatively consistent with previous pseudopotential calculations of the II rate in CdSe quantum dots[4], where the transition matrix elements of eq 1 were evaluated directly for $\hbar\omega \approx 2E_g$. In the case of a spherical CdSe quantum dot, 2.9 nm in diameter, the calculated II lifetime was $\tau^{II} = 76$ ps at $\hbar\omega \approx 2E_g$.[4]

The energy threshold $\hbar\omega_{th}$ for carrier multiplication is the minimum photon energy such that the photogenerated electron *or* the photogenerated hole have an excess energy $\Delta E_{h,e} \geq E_g$. The excess energy is defined as the difference between the electron (hole) energy and the conduction-band minimum (valence-band maximum) energy. It is easy to see that $2E_g < \hbar\omega_{th} < 3E_g$, as for $\hbar\omega < 2E_g$ the excess energy cannot be $> E_g$, whereas for $\hbar\omega > 3E_g$ the excess energy is always $> E_g$. Figure 4 shows the calculated total optical absorption spectrum of a 3.1-nm-diameter PbSe dot, as a function of the renormalized photon energy $\hbar\omega/E_g$. Also shown in Figure 4 is the XX-producing absorption spectrum, which includes only optical transitions that satisfy the conditions for II ($\Delta E_h > E_g$ or $\Delta E_e > E_g$). As we can see

from Figure 4, the XX-producing absorption spectrum has a well-defined energy threshold at $\hbar\omega_{th} \approx 2.2E_g$, indicating that carrier multiplication can be initiated by photons of this energy. We note, however, that for $\hbar\omega = 2.2E_g$ only about $^1/_4$ of the absorbed photons are potentially useful for II (ratio between the XX-producing absorption spectrum and the full absorption spectrum in Figure 4). This reduces the carrier-multiplication efficiency compared to $\hbar\omega = 3E_g$. Our calculated carrier-multiplication threshold is in agreement with the experimental observations of Ellingson et al.,[6] without the need, however, to invoke optically forbidden transitions. We find that the low-energy threshold is due instead to the asymmetry between the valence-band and conduction-band densities of states (Figure 2a), which allow optical transitions where the excess energy of the electron is significantly larger than that of the hole.

Our calculations show (Figure 3) that, for energies above $\sim 2.2E_g$, the intrinsic II rate ($X \rightarrow XX$) is much faster than the AR rate ($XX \rightarrow X$). However, the II decay channel competes with other radiative (e.g., electron−hole recombination) and nonradiative (e.g., electron/hole phonon-assisted cooling) decay paths for the photogenerated exciton. Radiative recombination times in PbSe quantum dots are rather long (>1 ns). Nonradiative intraband relaxation times ranging between 0.25 and 6 ps have been reported in the literature.[19,20] For exciton energies just above threshold ($\hbar\omega \approx 2E_g$), intraband relaxation is faster than II, leading to relatively small[6] or negligible[7] carrier multiplication efficiencies. For $\hbar\omega \approx 3E_g$, however, II is significantly faster than any competing decay processes and represents the main decay channel for an electron−hole pair of that energy (Figure 1). For even higher excitation energies, multiple carrier generation can occur through a chain process, whereby the bi-exciton generated by the II process decays into a tri-exciton, and so on. The physical reason for the ultrafast II decay rate lies in the very sharp increase of the multi-exciton DOS with energy (see Figure 2b). This is likely to be a common feature of many semiconductor quantum dots, suggesting that ultrafast II rates can be expected in other materials as well. Indeed, efficient carrier multiplication has been reported recently in CdSe,[7,8] PbS,[6] and PbTe[21] quantum dots.

In summary, we have proposed that the impact ionization mechanism can explain carrier-multiplication phenomena recently observed in PbSe colloidal nanocrystals and that no alternative models are required to explain existing experimental observations of (i) ultrafast carrier-multiplication rates (<200 fs)[5,6] and (ii) low-energy carrier-multiplication thresholds ($\hbar\omega < 3E_g$).[6] In the case of 3.1-nm-diameter PbSe quantum dots, our pseudopotential calculations predict a II threshold $\hbar\omega_{th} \approx 2.2E_g$ and a II lifetime smaller than 20 fs for $\hbar\omega \geq 3E_g$.

Acknowledgment. This work was supported by the U.S. Department of Energy, Office of Science, Basic Energy Sciences, under contract No. DE-AC36-99GO10337.

References

(1) Hoffert, M. I.; Caldeira, K.; Benford, G.; Criswell, D. R.; Green, C.; Herzog, H.; Jain, A. K.; Kheshgi, H. S.; Lackner, K. S.; Lewis, J. S.; Lightfoot, H. D.; Manheimer, W.; Mankins, J. C.; Mauel, M. E.; Perkins, L. J.; Schlesinger, M. E.; Volk, T.; Wigley, T. M. L. *Science* **2002**, *298*, 981.
(2) Nozik, A. J. *Physica E* **2002**, *14*, 115.
(3) Califano, M.; Zunger, A.; Franceschetti, A. *Nano Lett.* **2004**, *4*, 525.
(4) Califano, M.; Zunger, A.; Franceschetti, A. *Appl. Phys. Lett.* **2004**, *84*, 2409.
(5) Schaller, R. D.; Klimov, V. I. *Phys. Rev. Lett.* **2004**, *92*, 186601.
(6) Ellingson, R. J.; Beard, M. C.; Johnson, J. C.; Yu, P.; Micic, O. I.; Nozik, A. J.; Shabaev, A.; Efros, Al. L. *Nano Lett.* **2005**, *5*, 865.
(7) Schaller, R. D.; Agranovich, V. M.; Klimov, V. I. *Nat. Phys.* **2005**, *1*, 189.
(8) Schaller, R. D.; Petruska, M. A.; Klimov, V. I. *Appl. Phys. Lett.* **2005**, *87*, 253102.
(9) Schaller, R. D.; Klimov, V. I. *Phys. Rev. Lett.* **2006**, *96*, 097402−1.
(10) Guyot-Sionnest, P. *Nat. Mater.* **2005**, *4*, 653.
(11) Kolodinski, S.; Werner, J. H.; Wittchen, T.; Queisser, H. J. *Appl. Phys. Lett.* **1993**, *63*, 2405.
(12) Shockley, W.; Queisser, H. J. *J. Appl. Phys.* **1961**, *32*, 510.
(13) Werner, J. H.; Kolodinski, S.; Queisser, H. J. *Phys. Rev. Lett.* **1994**, *72*, 3851.
(14) Allan, G.; Delerue, C. *Phys. Rev. B* **2006**, *73*, 205423.
(15) Wang, L. W.; Califano, M.; Zunger, A.; Franceschetti, A. *Phys. Rev. Lett.* **2003**, *91*, 056404.
(16) Kang, I.; Wise, F. W. *J. Opt. Soc. Am. B* **1997**, *14*, 1632.
(17) An, J. M.; Franceschetti, A.; Dudiy, S. V.; Zunger, A. Unpublished work.
(18) Efros, Al. L.; Kharchenko, V. A.; Rosen, M. *Solid State Commun.* **1995**, *93*, 301.
(19) Schaller, R. D.; Pietryga, J. M.; Goupalov, S. V.; Petruska, M. A.; Ivanov, S. A.; Klimov, V. I. *Phys. Rev. Lett.* **2005**, *95*, 196401.
(20) Harbold, J. M.; Du, H.; Krauss, T. D.; Cho, K. S.; Murray, C. B.; Wise, F. W. *Phys. Rev. B* **2005**, *72*, 195312.
(21) Murphy, J. E.; Beard, M. C.; Norman, A. G.; Ahrenkiel, S. P.; Johnson, J. C.; Micic, O. I.; Ellingson, R. J.; Nozik, A. J. *J. Am. Chem. Soc.* **2006**, *128*, 3241.

NL0612401